



An Investigation On: Kinetics of Photo Catalysis, Electrical Property And Biological Activity of Electrochemically Synthesized ZnS And Ru: ZnS Nano Photocatalysts

K.R.Raksha and Sannaiah Ananda*

*Department of Studies in Chemistry, Manasagangotri, University of Mysore, Mysore-570 006, **INDIA**

Email: snananda@yahoo.com

Accepted on 7th January 2014

ABSTRACT

Zinc sulphide is one of the important II-VI semiconducting materials with a direct band gap of 3.8eV which finds applications in electrical conductivity and photocatalysts. This article deals with the novel electrochemical synthesis of ZnS and Ru: ZnS nano particles, their application in photocatalysts and electrical conductance. The synthesized nano particles were characterized by UV-VIS, IR, FE-SEM (EDAX) techniques. X-ray diffraction (XRD) reveals average crystallite size to be 19 nm and 12.7nm respectively. The photo-catalytic decolourization of the dye follows first-order kinetics. The photo-degradation efficiency for the synthesized nano particles was observed to be ~6-8 times greater than commercial ZnS and ZnO, studied with respect to change in COD. Resistivity measurements demonstrate that the electrical properties of the nanoparticles depend significantly on the content. The hydroxyl radical scavenging activity of ZnS and Ru: ZnS nano particle was established by Fenton reaction. The anti-bacterial effect of these particles against Bacillus subtilis and E. coli was investigated.

Keywords: Photocatalysis, Fenton reaction, Photovoltaic.

INTRODUCTION

ZnS is a key material for ultraviolet light-emitting diodes, injection lasers, cathode ray tubes, flat panel displays, and IR windows. It has a wide band gap of 3.8 eV at room temperature and has important luminescent properties and photocatalyst applications [1,2]. There are many works where ZnS nanoparticles are synthesized by other methods like mechanochemical and solvothermal techniques but ZnS obtained by these techniques have a wide band gap of 4- 4.6eV [3]. An electrochemical procedure, based on the dissolution of a metallic anode in a protic solvent, has been used to obtain nanoparticles ranging from 10 to 20 nm with reduced band gap. This is achieved by passing an electric current between two or more electrodes separated by an electrolyte. By definition, the synthesis takes place at the electrode – electrolyte interface [4,5]. Some of the advantages of this method are the high purity of the particles and the possibility of a precise particle-size (due to decrease in band gap) control achieved by adjusting the current density [6]. For the optimization, it is necessary to take into account the following parameters: the choice of the right solvent, supporting electrolyte, type of electrode, and the current density [7,8]. In recent

years, researchers have focused on the combination of different kinds of metallic oxide particles and metal ions. Studies have showed that Ru/CeO₂, Ru/TiO₂, Ru/ZnO and RuO₂-Zr/Na₂Ti₆O₁₃ were observed to be very active catalysts in many applications [9-12]. The characteristics and concentrations of dopants are responsible for particular properties and efficiencies of semiconductor nanoparticles. Hence investigation of the role of dopant concentration on photocatalytic, optical and electrical properties of doped semiconductor nanoparticles is very important from the viewpoints of basic physics as well as applications. Textile industries are one of the major contributors of hazardous organic pollutants like dyes into water bodies [12]. Removal of colour and organics by photocatalytic degradation is emerging as an effective treatment technique [15, 16]. Sulphur compounds prevent oxidative damage from Cu⁺ or Fe²⁺, and this observed antioxidant activity occurs at biological concentrations by metal coordination [17]. Studies have shown that zinc complex acts as hydroxyl radical scavenger [18, 19]. Therefore to study whether ZnS and Ru: ZnS nano particles could scavenge hydroxyl radical is of great significance. Because of the wide application of nano metal sulphides in various electrical fields [20- 22], impedance analysis of the samples was carried out to reveal the variation of impedance with frequency at room temperature. These results shows the capacitive admittance associated with the nanoparticles and hence nanostructure ZnS and Ru: ZnS can have potential applications in the electronics as nano-tuned devices in which resonant frequency can be adjusted by controlling the size and shape of the nanoparticles [2].

MATERIALS AND METHODS

Zinc metal, Sodium selenite, Sodium sulphide from Alfa –Aesar pvt ltd. Platinum electrode from Elico pvt ltd. Ruthenium chloride from Arora-Matthey ltd. All chemicals were used without further purification. Deionised water produced by a PURELAB Ultra water purification system was used for all the experiments.

Synthesis of ZnS nano particles: Nanoscaled ZnS was synthesized by an electrochemical process using zinc electrodes in an aqueous system with sodium sulphide as a conductive salt. The sodium sulphide was employed as the sulphur source. An electrochemical process based on an electrolytic cell was used. Platinum and zinc were used as electrodes with a lateral distance of 1.5 cm. They were fixed in a holder so that they were completely enclosed by the electrolyte. The electrochemically generated S²⁻ species reacted with Zn²⁺ in the electrolyte to produce ZnS nano particles. A potential difference of 1.7 V was applied between the electrodes by using a DC source. The synthesis was performed galvanostatically, at current density, j , of 80.0 mA cm⁻², with constant stirring (200 rpm), at room temperature for 3 h at a pH 6.0. The E/C synthesis of nanocrystals of Zinc sulphide involves two steps, as shown in Fig. 1: first, zinc is electrochemically deposited on electrode surface from an aqueous solution containing the zinc ion, second, these particles gets oxidized to give Zn²⁺ and react with S²⁻ species to yield nano particle of semiconducting ZnS. Finally, thus formed nano particles was washed repeatedly with distilled water until sodium sulphide is completely removed, centrifuged and calcinated at 750^oc for 2 hr to remove sodium and hydroxide impurities which has formed due to electrolysis and atmospheric oxidation.

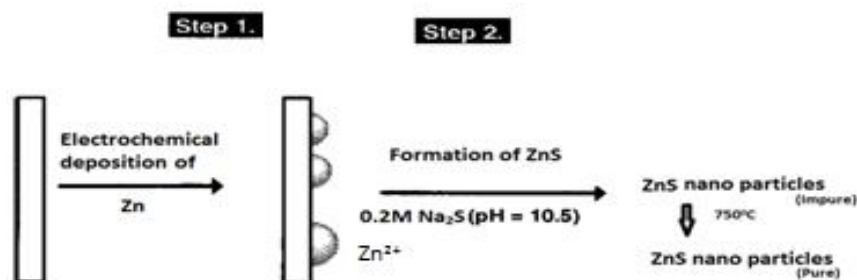
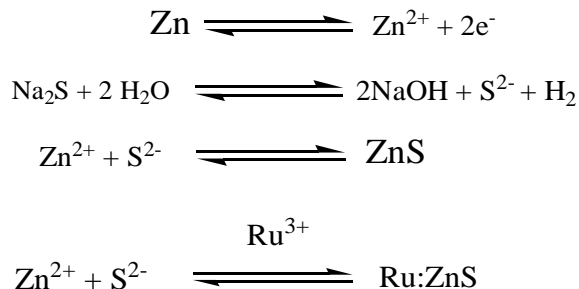


Fig. 1: Diagrammatic representation of electrochemical synthesis of ZnS nano particles

Synthesis of Ru: ZnS nano particles: The experimental set up is similar to synthesis of ZnS. Here, zinc and ruthenium coated platinum electrodes were used as anodes. The rate of electrochemical reaction is not same for Ru^{3+} and Zn^{2+} , as the redox potential of Ru^{3+} and Zn^{2+} are different. The rate of dissolution for Zn (-0.7618 V) is faster than Ru (0.68V), so that higher proportion of ZnS is formed where as Ru^{3+} opts to occupy interstitial lattice and at the surface of ZnS to give nano particles of Ru:ZnS. The mechanism of electrochemical formation of ZnS is as follows:



Characterization: The SEM images of the samples were recorded on ESEM Quanta-200 FEI-Netherlands, A scanning electron microscope. FT-IR spectra were recorded using JASCO FT-IR: 460plus with wave number ranging from 4000- 500 cm^{-1} . The optical absorption spectra have been observed by UV-Visible spectrophotometer at room temperature with JASCO- UV VIS spectrophotometer. For measuring the absorption characteristics, nanopowder is first dispersed in isopropyl alcohol (IPA) and then taken in a quartz cuvette of path length of 10 mm. The powder X-ray diffraction patterns were recorded using Rigaku miniflex II desktop X-ray diffractometer (Cu-K radiation, $\lambda = 1.54\text{\AA}$) employing a scan rate of $0.02^\circ/\text{s}$ range from 0° to 60° . Impedance measurement is done using Zhanher IM6 LCR meter.

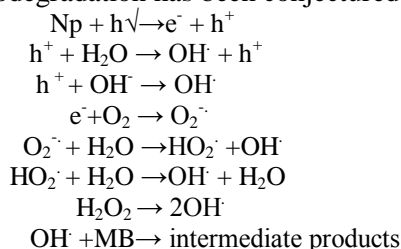
Mineralization of dye: The dopant, pH of solution, dosage of photo catalyst, concentration of dye and exposure to different source of light viz, sunlight and UV light are variables that influence on the photo reactivity of nanocatalysts ^[11,16]. To assess the photocatalytic efficiency of the prepared nano particles, photodegradation experiments were carried out using different concentration of Indigo carmine dye as substrate and different concentrations of ZnS and Ru: ZnS as catalyst. A calculated quantity of the catalyst was added to the dye solution, stirred in the dark for 1 min to establish adsorption/desorption equilibrium between the dye and nano particle molecules and then illuminated under 8W UV source to induce a photochemical reaction. Aliquots were taken at an interval of 2/5 min determined by Elico SL 171 mini spectrometer. Adsorption and the photocatalytic conversion (g %) was calculated as follows [14]:

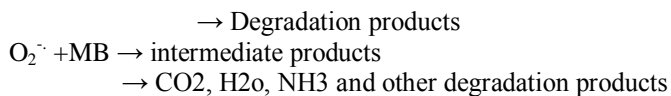
$$\text{COD} = \frac{8000 (\text{vol of FAS in blank} - \text{vol of FAS in dye soln}) \text{ normality of FAS}}{\text{sample volume}}$$

The mineralization of dye was measured by the decrease of chemical oxygen demand (COD) of the solution. COD was measured according to the standard dichromate titration method. The mineralization efficiency of dye was estimated by the following expression [14]

$$\% \text{ efficiency} = \frac{\text{final COD} - \text{initial COD}}{\text{final COD}} \times 100$$

The mechanism of photodegradation has been conjectured as seen in Scheme (1) ^[13, 23]





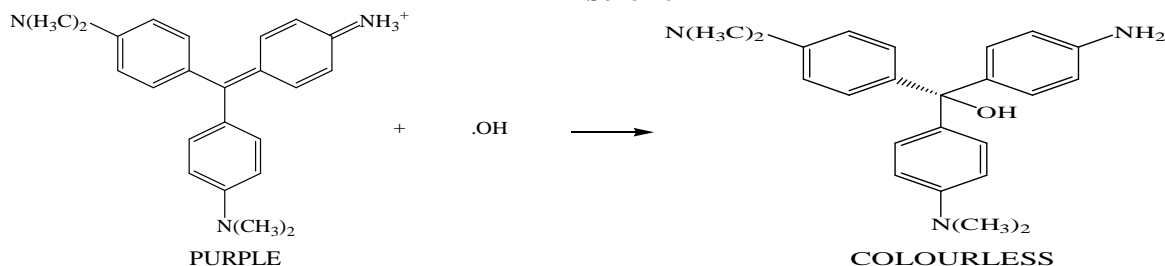
Scheme 1

Photo-voltaic and impedance measurements: To measure the conductivity and potential, the particles is embedded into a glass tube of diameter 1cm and length 5 cm by mechanical pressing. The ends of the glass tube containing nanoparticles is connected through two copper wires to a conductometer (Elico CM 180) to measure the conductivity in presence of UV light, sunlight and without light (Table. 6). Same procedure is followed to measure the potential using potentiometer (Equip-Tronics EQ-606). Electrical property is further confirmed by impedance measurement which is a powerful method of characterizing many of the electrical properties of materials and their interfaces with electronically conducting electrodes^[20, 21,22]. Resistance is recorded at room temperature in the frequency range from 1Hz to 1MHz.

Free radical scavenging activity: It is known that methyl violet (MV) has a maximum absorption (λ_{max}) at 582 nm. A Fenton reaction is an oxidative reaction in which the generated hydroxyl radical can react with MV by attacking its $-\text{C}=\text{C}-$ where it has highest electron cloud, leading purple MV into a colourless product, correspondingly its absorption decreases^[24]. The change of absorbance (denoted as ΔA) directly indicates the amount of $\bullet\text{OH}$ generated. Larger the ΔA value, higher is the $[\bullet\text{OH}]$. When a certain amount of synthesized nano metal sulphide and commercial ZnS is added to the Fenton system, if our synthesized metal sulphide nano particle is able to eliminate $\bullet\text{OH}$, part of the MV will be protected from being attacked, therefore there will be increase in absorbance and ΔA will decrease. The reaction mechanism of hydroxyl radical scavenging has been conjectured as seen in the following reactions [24]:



Scheme 2



Experimental: In the present work, the suspended solution of nano particle was prepared at a concentration of $10\mu\text{M}$ by dispersing in 0.1 M Tris- HCl, pH 4.7. The reaction mixture for photometric determination contains $1.2 \times 10^{-5}\text{M}$ MV, 0.15mM FeSO_4 , 1.0M H_2O_2 , 0.1M Tris- HCl buffer and appropriate nano particle in a final volume of 5ml. After incubation at room temperature for 5 min in the absence of UV light, the absorbance of the reaction solution was measured at 582nm.

Anti-bacterial activity: The synthesized ZnS and Ru: ZnS nanoparticles were tested for antibacterial activity by Disc diffusion method against Escherichia Coli, Bacillus subtilis and salmonella typhii. The pure bacterial culture was sub cultured on nutrient agar media. The activity was compared against standard Chloramphenicol. The concentration of nanoparticles was 0.5 mg/ml and 30 μl of each solution was placed on a disc. After incubation for 48 hrs at 37°C , the different levels of zone inhibition of bacteria were measured.

RESULTS AND DISCUSSION

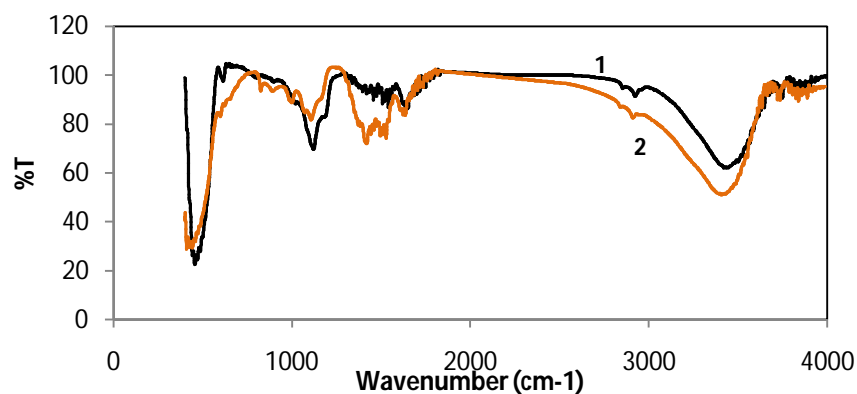


Fig. 2: FTIR spectra of 1. ZnS, 2. Ru: ZnS nano particles

The IR spectra for ZnS and Ru: ZnS nanoparticles are shown in fig.2. Formation of ZnS can be justified by the presence of a sulphur and zinc stretching frequencies in the region $500\text{-}600\text{cm}^{-1}$ and 1200cm^{-1} respectively [1]. The formation of Ru: ZnS [9] was evident by the presence of ruthenium stretching frequency at $1400\text{-}1500\text{cm}^{-1}$

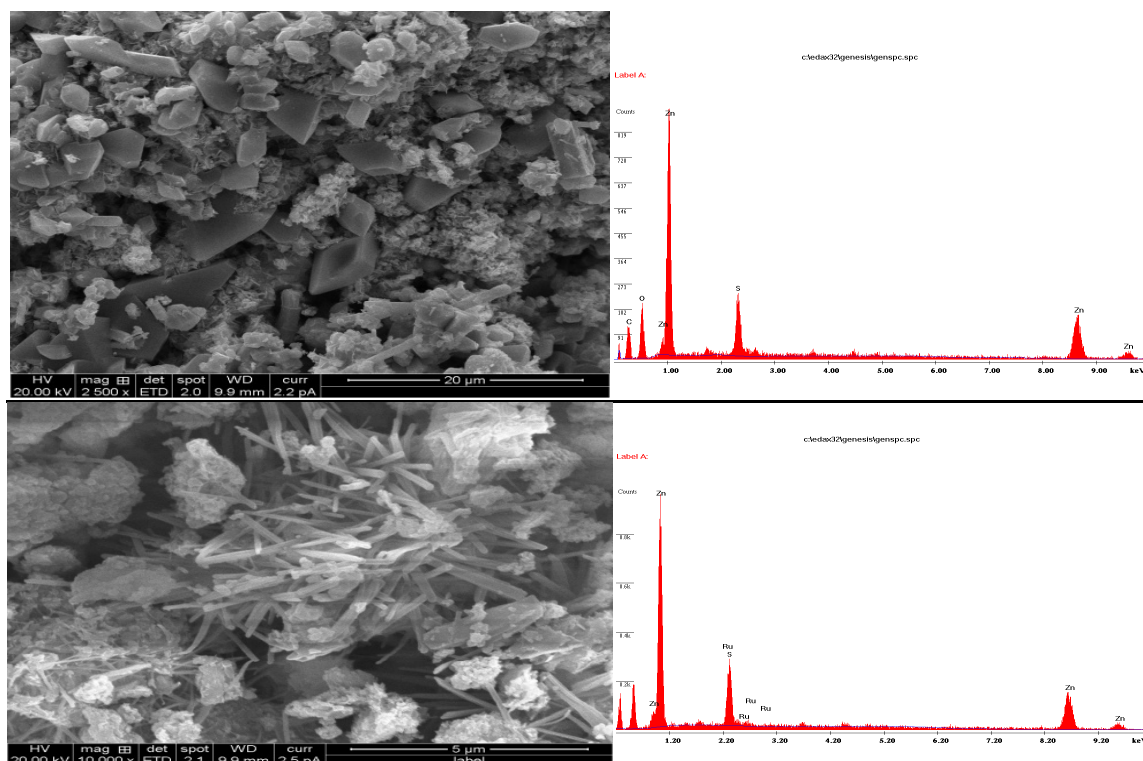


Fig. 3 SEM and EDAX of ZnS and Ru:ZnS nanoparticles

The morphology of ZnS and Ru: ZnS were investigated by FE-SEM shown in Fig. 3. It can be found from the figure. 3 that the surface of ZnS includes particle cluster distributed unevenly. However, in case of Ru: ZnS some nano rod with cluster-like structure was observed. From the EDAX analysis, the presence of zinc and sulphur in ZnS and ruthenium along with zinc and sulphur in Ru: ZnS were confirmed. The higher intensity for Zn compared to Ru reveals doping of ruthenium to ZnS.

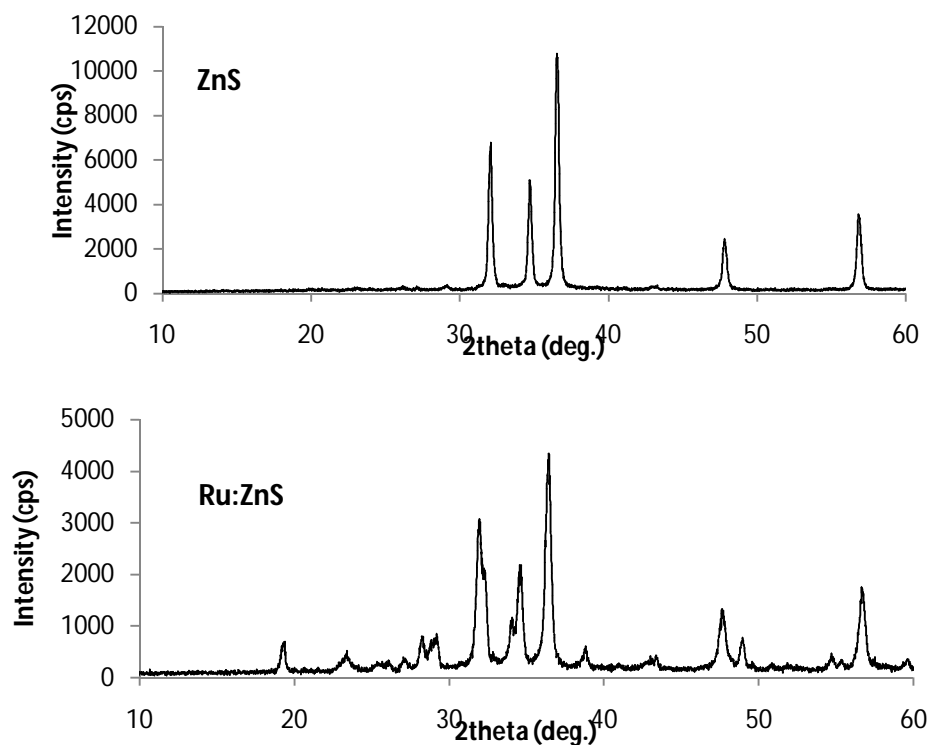


Fig. 4: XRD and W-H plot of ZnS and Ru: ZnS nanoparticles

XRD pattern of the prepared ZnS and Ru: ZnS nanoparticles samples are shown in fig.4. XRD for ZnS shows three main diffraction peaks at 2θ values 32.05, 33.8 and 36.5. The peaks are appearing due to reflection from the (310), (311) and (203) planes of the cubic phase of the ZnS [2]. The obtained peak positions correspond to zinc blended type patterns. The XRD pattern of the nanocrystal is well matched with the standard cubic ZnS. For Ru: ZnS in addition to ZnS peaks, peaks at 19.2(003) and 23.4(221) were observed which corresponds to Ru: ZnS [8]. The average crystallite size of the ZnS and Ru: ZnS nanoparticles as calculated using Debye Scherrer equation is 19 nm and 12.7nm respectively, both with the structure tetragonal. The angle strain is measured to be 1.42×10^{-3} for ZnS and 5.8×10^{-4} for Ru: ZnS. It is further confirmed by Williamson Haal plot which is a plot of $4\sin \theta$ vs. $\beta\cos \theta$ where intercept gives the crystallite size and slope gives the angle strain [26].

Optical absorption and optical band gap: From the optical absorption spectra it is clear that maximum absorption for ZnS is at 305nm and for Ru: ZnS is 220 nm. This peak position reflects the band gap of particles. There is no absorption peak at visible region. The direct band gaps of the sample are calculated using Tauc's plot[27,10] by plotting $(\alpha h\nu)^{1/2}$ vs. $h\nu$ and then extrapolating the straight portion of the curve on $h\nu$ axis at $a = 0$, shown in Fig. 5 and found to be 2.6eV for ZnS and 3.8eV for Ru:ZnS. The obtained value of the band gap of ZnS nanoparticle is lower than that of the bulk value of ZnS (3.68 eV). The wide energy gap (2.6 and 3.8 eV) limits their application to UV region. This blue shift of the band gap of ZnS nano particle takes place because of the quantum confinement effect. The higher band gap of Ru: ZnS supports lower photocatalytic activity compared to ZnS.

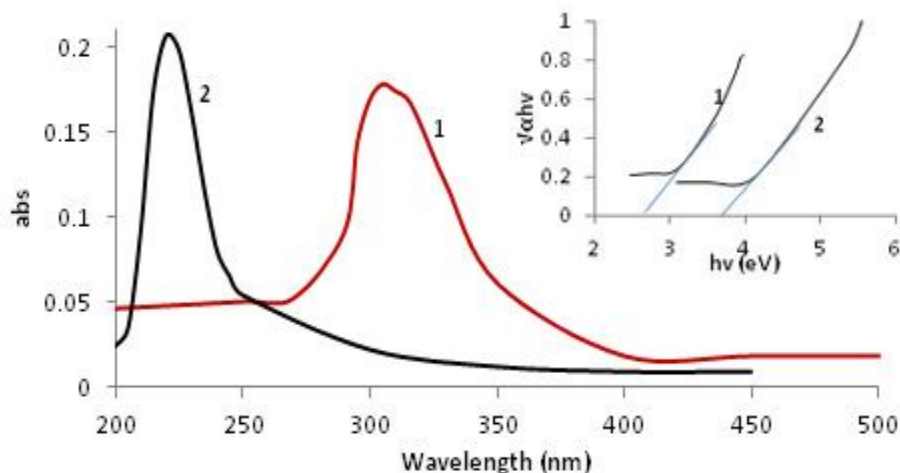


Fig. 5: UV-VIS spectra of 1.ZnS, 2.Ru: ZnS nanoparticles **Inset:** Tauc's plot

Photo-catalytic degradation of Indigo carmine dye

Effect of catalyst loading: Table 3 shows the rate constant of degradation with respect to different concentration of catalyst. Several studies have indicated that the photocatalytic rate initially increases with catalyst loading and then decreases at high values because of light scattering and screening effects^[15] The tendency toward agglomeration (particle-particle interaction) also increases at high solids concentration, resulting in a reduction in surface area available for light absorption and hence a drop in photocatalytic degradation rate [14]. Although the number of active sites in solution will increase with catalyst loading, a point appears to be reached where light penetration is compromised because of excessive particle concentration. A further increase in catalyst loading beyond the optimum will result in non-uniform light intensity distribution, so that the reaction rate would indeed be lower with increased catalyst dosage. In this work, a high efficiency at mere low concentration of catalyst was achieved at 0.02g of catalyst for both ZnS and Ru: ZnS nanoparticles (Fig. 6).

Table 1: Effect of catalyst loading on the rate of photo-degradation

Nano particle	Amount of Catalyst/ 20ml	k sec ⁻¹	Time taken for complete degradation (min)	COD values in mg/l		Degradation efficiency %
				Before degradation	After degradation	
Commercial ZnS	0.02g	1.5×10^{-4}	92	352	288	1.8
Blank	-----	0.61×10^{-4}	--	352	336	0.45
Zinc sulphide	0.02g	11.9×10^{-4}	22	352	16	95.4
	0.04g	11.4×10^{-4}	22	352	16	95.4
	0.06g	10.9×10^{-4}	22	352	32	90.9
Ruthenium doped Zinc sulphide	0.02g	5.5×10^{-4}	35	352	32	90.9
	0.04g	1.6×10^{-4}	90	352	32	90.9
	0.06g	1.0×10^{-4}	115	352	32	90.9

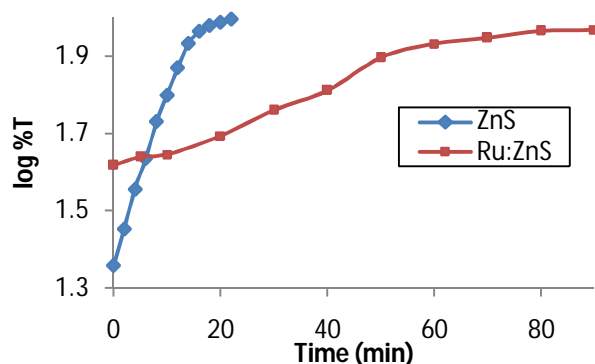


Fig 6: Plot of log %T vs. time for ZnS and Ru: ZnS

Effect of concentration of dye: Degradation is carried out in different concentration of dye (Table. 2). As the optimum catalyst concentration for ZnS nano particle is 0.02g, keeping this as standard the same amount of Ru: ZnS nano particle is taken for comparison in the further work. As the initial concentration of dye increases, the degradation efficiency reduces (Fig. 7). The possible reason is that, as initial concentration of dye is increased; more dye molecules are adsorbed onto the surface of the catalyst. but the adsorbed dye molecules are not degraded immediately because the intensity of the light and the catalyst amount is constant and also the light penetration is less. Also with the increase in the dye concentration, the solution becomes more intense coloured and the path length of the photons entering the solution is decreased thereby fewer photons reached the catalyst surface [14, 15]. Hence the production of hydroxyl and superoxide radical efficiency is reduced.

Table 2: Effect of concentration of dye on the rate of degradation

Catalyst 0.02g	Concentration of dye (M)	k sec ⁻¹	Time taken for complete degradation (min)	COD values in mg L ⁻¹		Degradation efficiency %
				Before degradation	After degradation	
Zinc sulphide	0.2×10 ⁻⁴	6.6×10 ⁻⁴	22	304	48	86
Ruthenium doped Zinc sulphide	0.2×10 ⁻⁴	1.6× 10 ⁻⁴	90	304	32	90.9
Zinc sulphide	0.5×10 ⁻⁴	4.4× 10 ⁻⁴	90	752	32	90.9
Ruthenium doped Zinc sulphide	0.5×10 ⁻⁴	2.6× 10 ⁻⁴	140	752	32	90.9

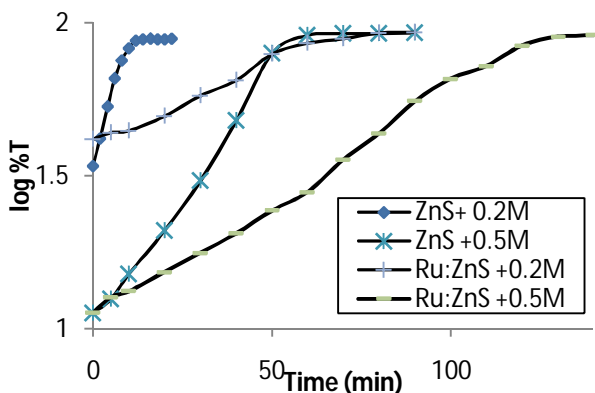


Fig 7: Plot of log %T vs. time with respect to different initial concentration of dye

Effect of temperature: Increase of temperature indicates slighter increase in the rate of photodegradation as raise in temperature results in increase of number of effective collisions leading to higher rate of reaction (Fig. 8). However, the photodegradation efficiency is not much affected (Table 3).

Table 3: Effect of temperature on degradation of dye

Catalyst 0.02g	Temp °c	Concentr ation of dye (M)	k sec ⁻¹	Time taken for complete degradatio n (min)	COD values in mg/l		Degradatio n efficiency %
					Before degradatio n	After degradati on	
Zinc sulphide	50	0.2×10 ⁻⁴	13.5×10 ⁻⁴	10	352	16	95.4
	65	0.2×10 ⁻⁴	15×10 ⁻⁴	12	352	16	95.4
Rutheniu m doped Zinc sulphide	50	0.2×10 ⁻⁴	6.6×10 ⁻⁴	20	352	32	90.9
	65	0.2×10 ⁻⁴	9.8×10 ⁻⁴	16	352	32	90.9

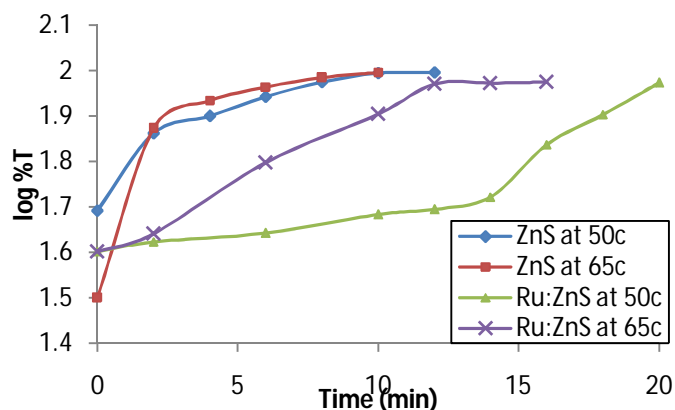


Fig 8: Plot of log %T vs. time with respect to different temperature

Reusability and regeneration: The re-use sample has shown almost same degradation efficiency compared to the fresh samples (Fig. 9). This indicates the nano samples can be regenerated and re-used with very low or insignificant change in the efficiency. While an obviously decrease in rate of reaction was noticed with the second use of catalyst (Table. 4). Reuse cycles might cause the aggregation of photocatalyst and the decrease in specific surface area and the losses of catalyst, resulting in a loss of catalytic activity.

Table 4: Efficiency of catalyst in second use

Catalyst 0.02g	Concentratio n of dye (M)	k sec ⁻¹	Time taken for complete degradation (min)	COD values in mg/l		Degradation efficiency %
				Before degradation	After degradatio n	
Zinc sulphide	0.2×10 ⁻⁴	1.8×10 ⁻⁴	90	352	16	95.4
Ruthenium doped Zinc sulphide	0.2×10 ⁻⁴	1.3×10 ⁻⁴	135	352	16	95.4

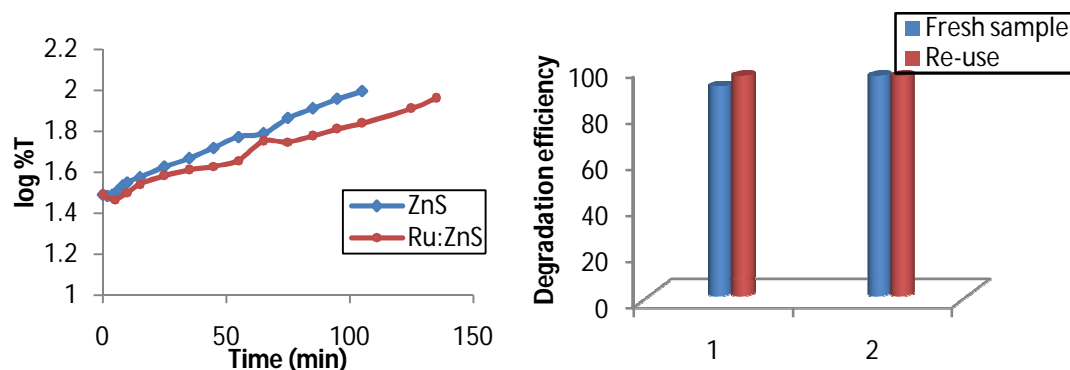


Fig 9a: Kinetics of photodegradation of re-use of catalyst. **9b:** Comparison of efficiency of fresh samples with re-use 1.ZnS 2.Ru: ZnS

Degradation in sunlight: The suspension of nano catalyst in dye was irradiated with sunlight and the photocatalytic experiments were conducted in July 2013, over a continuous 5 day period. All experiments were done in an open atmosphere between 9:30 a.m. and 2.30 p.m. The solar intensity fluctuations were minimal, and the mean illumination of sunlight is 96000 lux. Simultaneously, the catalytic studies were on all the different samples done in parallel in order to minimize the impact of fluctuations in daylight intensity. As the maximum absorption of both ZnS and Ru: ZnS is in UV region, rate of degradation is very much low (table.5) but the efficiency of degradation is not affected (Fig. 10).

Table 5: Effect of rate of degradation in sunlight

Catalyst 0.02g	Concentration of dye (M)	k sec ⁻¹	Time taken for complete degradation (min)	COD values in mg/l		Degradation efficiency %
				Before degradation	After degradation	
Zinc sulphide	0.2×10^{-4}	3.3×10^{-4}	90	352	16	95.4
Ruthenium doped Zinc sulphide	0.2×10^{-4}	1.5×10^{-4}	90	352	16	95.4

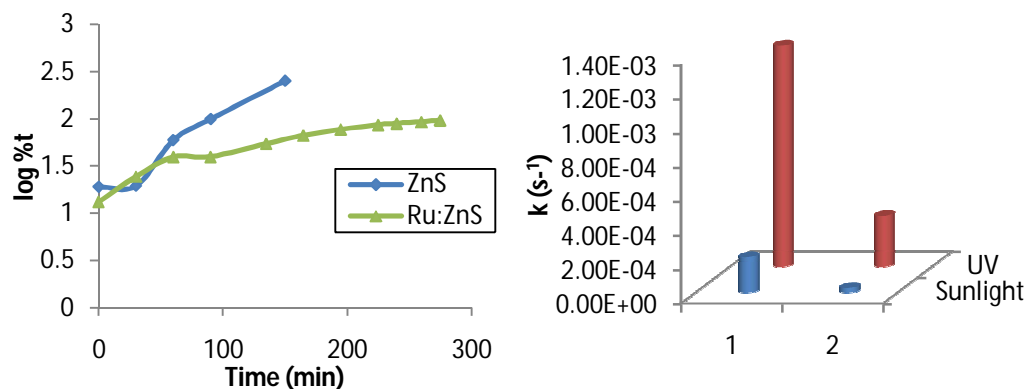


Fig 10a: Kinetics of photodegradation in sunlight. **10b:** Comparison of rate in UV light with sunlight 1.ZnS 2Ru: ZnS

Photo-voltaic activity of Catalysts:

Table 6: Measurement of potential and conductivity of ZnS, Ru: ZnS nano particles

Property	Catalyst	Dark	Sunlight	U-V
Potential measurements in mV	Commercial ZnO	1.0	20	40
	Commercial ZnS	1.0	10	40
	ZnS	1.0	83	89
	Ru:ZnS	0.0	58	60
Conductivity measurements in μS	Commercial ZnO	1.3	8.6	7.2
	Commercial ZnS	1.4	8.8	7.2
	ZnS	1.8	16.3	18.2
	Ru:ZnS	1.6	16.1	17.4

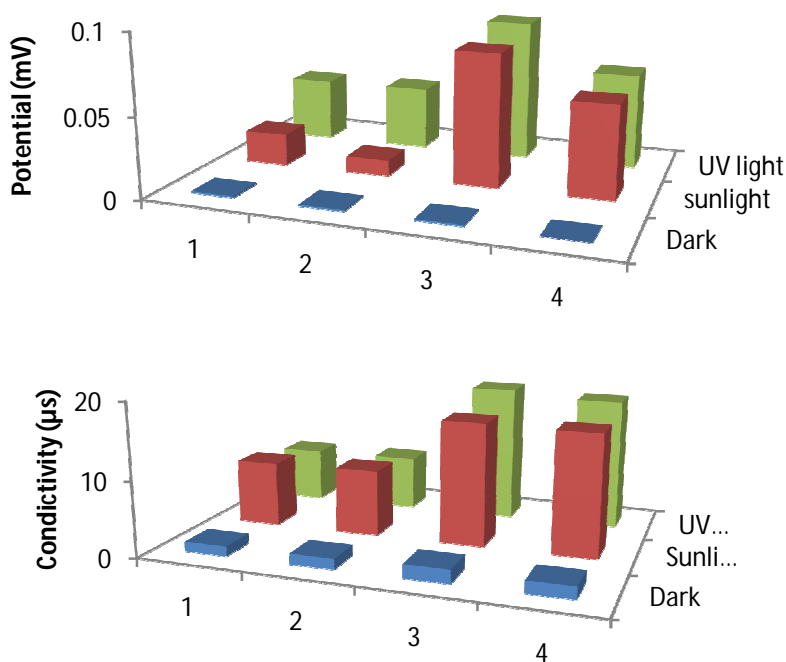
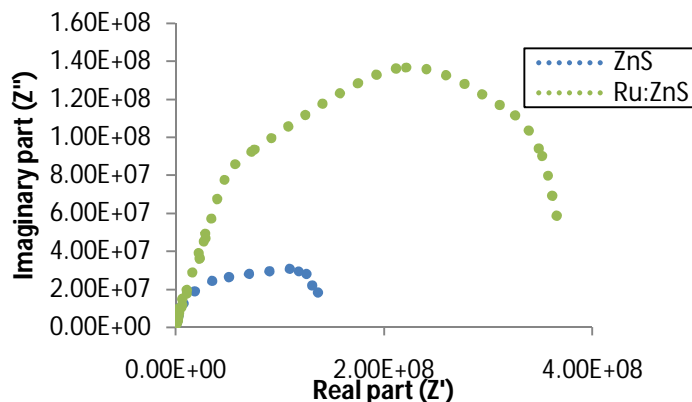


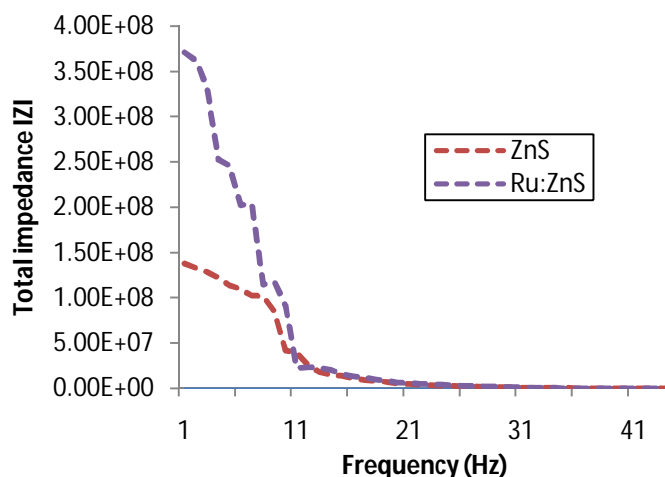
Fig 11: Potential and Conductivity measurements of 1.Commercial ZnO 2.Commercial ZnS 3. Nano ZnS 4. Nano Ru: ZnS

Compared to commercial samples, the photo-voltaic activity of ZnS nanoparticles is enhanced 8-10 times and approximately 6 times for Ru: ZnS nanoparticles in presence of sunlight and UV light (Table 6). The measurement of conductivity in presence UV light indicates Ru:ZnS as less photocatalytic than ZnS (Fig. 11).

Impedance studies:**Fig 13:** Nyquist plot of nano ZnS and nano Ru: ZnS

The impedance measurement was performed in a frequency range from 1 Hz to 1 MHz using Zhanher IM6 LCR meter at room temperature. Fig. 13 shows Nyquist plot of ZnS and Ru: ZnS. Only a single semi-circle is obtained for both the samples. The size of the semicircle for ZnS is smaller than that for Ru: ZnS indicating the electrical resistance is in the order $ZnS < Ru: ZnS$. Improvement in crystallinity of Ru: ZnS can also be attributed to this decrease in resistivity.

Further, Fig.14 shows the Bode plot (variation of total impedance with frequency) for these samples [21]. The impedance values are typically higher in low frequency region and decreases gradually with increasing frequency. The value of $|Z|$ appears to merge in the high frequency region for the samples. Total impedance for ZnS is lower than Ru:ZnS. Therefore, the impedance study clearly indicates that synthesized ZnS is better photocatalyst compared to Ru: ZnS [22].

**Fig 14:** Bode plot of nano ZnS and nano Ru:ZnS**Free radical scavenging activity:**

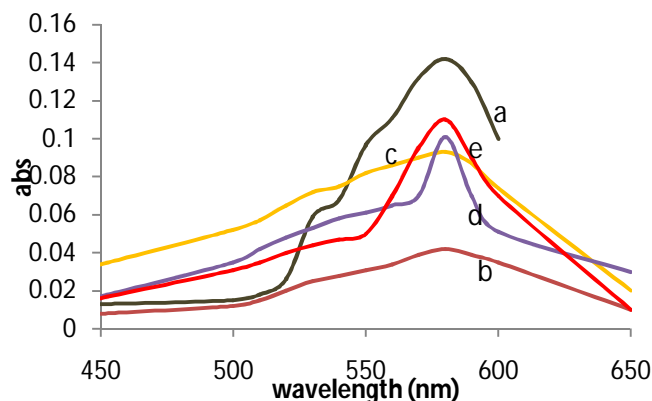


Fig15: UV-Vis absorption spectra of: a)MV, b)MV/FeSO₄/H₂O₂, c) MV/FeSO₄/H₂O₂/Nano ZnS d)MV/FeSO₄/H₂O₂/ Nano Ru:ZnS, e) MV/FeSO₄/H₂O₂/Com ZnS

The result (Fig. 15) indicates that after addition of metal sulphides, the absorbance partially increases and ΔA decreases, which proves that the synthesized metal sulphides and commercial ZnS indeed scavenges part of $\bullet\text{OH}$ and protects MV from further fading as a result[14]. Therefore, this photometric method is feasible to demonstrate the free radical scavenging activity of nano metal sulphides in comparison with commercial ZnS. The scavenging activity of nano particles were determined at different incubation times (Fig. 16). It can be seen that ΔA increases with incubation time from 5-15 min.

The probable mechanism of $\bullet\text{OH}$ scavenging activity of nano particles is shown in scheme (3). It can be seen that the reversible cycle between Zn^{+2} and Zn^{+3} imparts ZnS nanoparticles the protective activity that can maintain through the incubation time. After Zn^{+3} is converted back to Zn^{+2} , more $\bullet\text{OH}$ will be continuously scavenged. The more initial Zn^{+2} in the cycle, there is the more $\bullet\text{OH}$ can be scavenged. Therefore, higher scavenging activity is observed for commercial ZnS compared to synthesized ZnS, as ZnS nanoparticles may contain Zn^{+1} and ZnS^{+2} particles. Further, the doping of ruthenium to ZnS increases scavenging activity compared to ZnS nanoparticles due to increased band gap of Ru: ZnS (3.8eV).

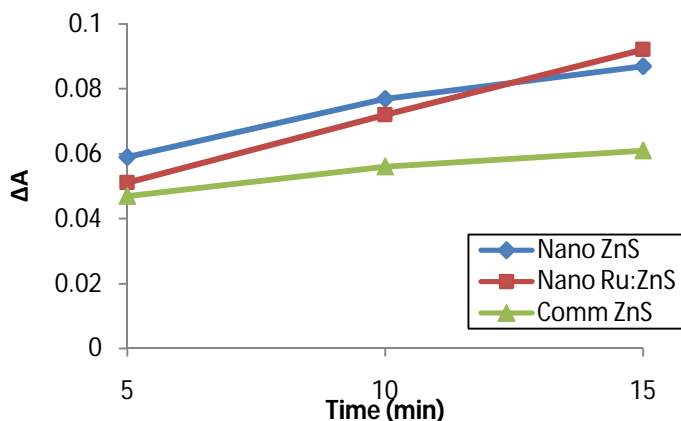
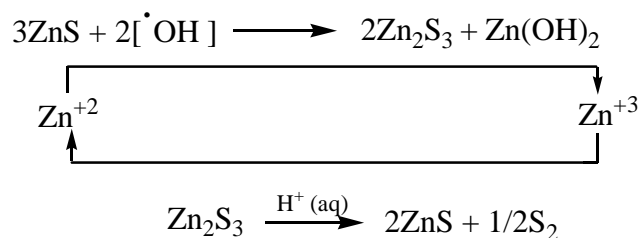
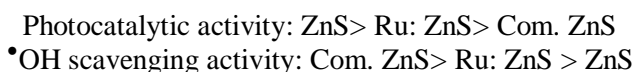


Fig. 16: Change of ΔA with incubation time in the reactive solutions

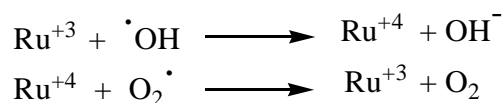


Scheme 4

The above results reveal that the increase of photocatalytic activity decreases $\cdot\text{OH}$ scavenging activity in the order:



When a photoactive material such as ZnS is doped with transition metal like Ru^{3+} , some of the Ru ions may be located at or near the surface of ZnS and can act as scavenger for free radicals [28]. Therefore, the doping reduced the photocatalytic activity [29]. Reaction that could result in the scavenging superoxide and hydroxyl radical are shown below (Scheme. 4)



Scheme 5

APPLICATIONS

Anti-bacterial activity:

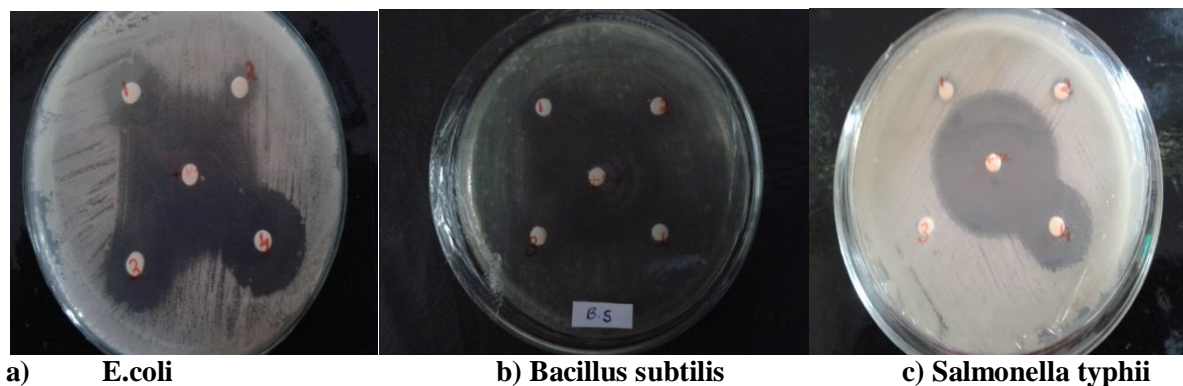


Fig 16: Anti bacterial activity of 1. ZnS and 2. Ru:ZnS nano particles against a) E. Coli b) Bacillus subtilis c) Salmonella typhii in comparison with the standard Chloramphenicol (+ve control)

Table 8: Anti-bacterial activity of synthesised nano particles against different strains of bacteria

Bacterial strain	Zone of inhibition (mm)		
	+ve control	ZnS	Ru:ZnS
E. coli	30	18	16
Bacillus subtilis	35	24	15
Salmonella typhii	32	0	5

There is a linear correlation between OH concentration and biological activity [30,31]. Ru: ZnS is an efficient OH scavenger (under the condition where OH radical production is inhibited) than ZnS, as a result Ru: ZnS exhibits low inhibition of bacterial growth. This explanation is consistent with the fact that zone of inhibition for bacterial growth is less for Ru: ZnS than that for ZnS.

CONCLUSIONS

Electrochemical method has shown good prospects in the controllable synthesis of small-sized nano materials. Moreover, the obtained particles have highly enhanced photocatalytic activity. Therefore, the simple, cost-effective, and eco-friendly synthetic method allows for its application in large scale production. The kinetics of photo degradation of dye shows that at 0.02g of catalyst, ZnS acts as a efficient photocatalyst in UV light compared to Ru: ZnS. Time taken for dye degradation, in case of ZnS nanoparticles is appreciably less which proves its high efficiency than ZnO. It is observed that Ru ions close to the surface can very well act as scavengers for free radicals and therefore, Ru:ZnS has higher hydroxyl radical activity and low photocatalytic activity. Both ZnS and Ru:ZnS shows considerable photovoltaic property and can have potential applications in the electronics. Synthesized nanoparticles show considerably good inactivation of different strains of bacteria.

ACKNOWLEDGEMENT

This work was funded by grants from Centres with Potential for Excellence in Particular Area (CPEPA), University of Mysore, India.

REFERENCES

- [1] Swarup KumarMaji, NillohitMukherjee, AnupMondal, Bibhutosh Adhikary, Basudeb Karmakar, *Journal of Physics and Chemistry of Solids*, **2011**,72 , 784–788
- [2] C.S. Pathak, M.K. Mandal, V. Agarwala, *Superlattices and Microstructures*, **2013**, 58 , 135–143
- [3] Ingrid Grobelsek, Benjamin Rabung, Mario Quilitz, Michael Veith, *J Nanopart Res*, **2011** 13,5103–5119
- [4] Won-Kyu Han, Jae-Woong Choi, Gil-Ho Hwang, Seok-Jun Hong, Jai-Sung Lee, Sung-Goon Kang, *Applied Surface Science*, **2006**, 252 , 2832–2838
- [5] L. Rodri´guez-Sa´nchez, M. C. Blanco, and M. A. Lo´pez-Quintela, *J. Phys. Chem. B*, **2000**, 104, 9683-9688
- [6] Cheonho Yoon and Jung Sang Suh, *Bull. Korean Chem. Soc.* **2002**, 23(11), 1519-1523
- [7] Hai Ming, Zheng Ma, Yang Liu, Keming Pan, Hang Yu, Fang Wang and Zhenhui Kang, *Dalton Transactions*, **2012**, 41, 9526
- [8] M. A. Anderson, S. Gorer, and R. M. Penner, *J. Phys. Chem. B*, **1997**, 101, 5895-5899
- [9] G. Chaitanya Lakshmi, S. Ananda, R. Somashekar, *International Journal of Advances in Science and Technology*, **2012**, 5 (2).
- [10] G. Chaitanya Lakshmi, S. Ananda, R. Somashekar and C. Ranganathiah, *International Journal of Advances in Science and Technology*, **2012**,5 (6).
- [11] V´azquez-Cuchilloa, R. G´omez, A. Cruz-L´opez, L.M. Torres-Mart´inez, R. Zanellad, F. J. Alejandra Sandovala, K. Del ´Angel-S´anchez, *Journal of Photochemistry and Photobiology A: Chemistry*, **2013**, 266 , 6– 11.
- [12] Ting-Ting Miao, Yuan-Ru Guo, Qing-Jiang, *Pan J Nanopart Res*, **2013**, 15, 1725.
- [13] N. Neelakandeswaria, G. Sangamia, N. Dharmaraja, Nam Ki Taekb, Hak Yong Kimb, *Spectrochimica Acta Part A* , **2011**,78, 1592–1598.

- [14] A K Subramani, K Byrappa, S Ananda, K M Lokanatha Rai C Ranganathaiah And M Yoshimura, *Bull. Mater. Sci.*, **2007**, 30(10), 37–41.
- [15] Yan Xiaojua, Bao Ruilinga, Yu Shuilib, Li Qiongfanga, and Jing Qingfeng, *Russian Journal of Physical Chemistry A*, **2012**, 86, (9), 1479–1485.
- [16] C. Coudray, S. Rachidi, A. Favier, *Biological trace element research*, **1993**, 38.
- [17] Erin E. Battin, E Julia L. Brumaghim, *Cell Biochem Biophys*, 2009, 55, 1–23.
- [18] W. H Bannister, J. V. Bannister, A.J. F. Searle and P.J Thornalley, *Inorganica Chimica Acta*, **1983**, 78, 139-142.
- [19] Carolyn I. Pearce, Richard A.D. Patric, David J. Vaughan, *Reviews in Mineralogy & Geochemistry*, **2006**, 61, 127-180.
- [20] S. Chellammal, S. Sankar, **2010**, 13(3), 214–216.
- [21] A U Ubale And D K Kulkarni, *Bull. Mater. Sci.*, **2005**, 28(1), 43–47.
- [22] B. L. Abrams and J. P. Wilcoxon, *Reviews in Solid State and Materials Sciences*, **2005**, 30, 153–182.
- [23] Ying Xue, Qingfen Luan, Dan Yang, Xin Yao, Kebin Zhou, *The journal of physical chemistry*, **2011**, 115, 4433-4438.
- [24] Ratan Das, Sneha Gang, Siddhartha Sankar Nath, *Journal of biomaterials and nanobiotechnology*, **2011**, 2, 472-475.
- [25] Joshua pelleg, e. Elish, and d. Mogilyanski, *Metallurgical and materials transactions a*, **2005**, 36a, 3187.
- [26] S H Mohamed, *J. Phys. D: Appl. Phys.* **2010**, 43, 035406.
- [27] Chengfang Li, Gongwu Song, *Sensors and Actuators B: Chemical*, **2009**, 137, 432-436
- [28] Marmion CJ, Cameron B, Mulcahy C, Fricker SP, *Pub med*, **2004**, 4(15), 1585-603
- [29] Javier Marugán, Rafael van Grieken, Cristina Pablos, Carlos Sordo, *Water Research*, **2010**, 44, 789-796.
- [30] Min Choa, Hyenmi Chungb, Wonyong Choic, Jeyong Yoon, *Water Research*, **2004**, 38, 1069–1077.